Spatial self-organization of a nanoscale structure on the Pt(111) surface

L. P. Zhang,* J. van Ek,† and U. Diebold‡
Department of Physics, Tulane University, New Orleans, Louisiana 70118
(Received 18 May 1998)

A self-organized nanostructure has been observed on the Cr/Pt(111) system. Cr overlayers with various coverages were deposited on a Pt(111) surface. Upon annealing to different temperatures, metastable surface alloys characteristic for a miscible metallic system have been observed. For a limited coverage range from 1.5 to 3.0 ML and an annealing temperature of 800 K, a spatial self-organization takes place on the bimetallic surface, forming a highly ordered hexagonal superstructure. The scanning tunnel microscope contrast of the superstructure is sensitive to the bias voltage, resulting in different patterns: either a mosaic structure and/or a network consisting of one-atom-wide lines. Relative to the Pt(111) surface, the superstructure has a $(\sqrt{39} \times \sqrt{39})R16.1°$ unit cell with a dimension of 17.3 Å. We propose that the network consists of Pt dislocation lines, and is caused by a stress-induced reconstruction of the top Pt(111) layer. The mosaic pattern is related to a two-dimensional array of Cr clusters containing only ten atoms. [S0163-1829(98)02547-8]

I. INTRODUCTION

Nanostructures are expected to exhibit potentially significant physical and chemical properties.[1] Periodic structures on the nanoscale may be fabricated by creating conditions favorable for self-organization. In heteroepitaxy, self-organization is driven by the relief of built-up stress and the tendency to reduce the chemical free energy of a surface. Various patterns of trenches and wires, as well as highly organized nanoscale arrays have been yielded during film growth of semiconductor systems.[2,3] The ''herringbone'' reconstruction of Au(111) surfaces acted as a template for the formation of well-ordered arrays of metal islands.[4–6] In the Co/Pt(111) system, a cause-and-effect relationship has been observed, that is, the strain associated with the growth and adsorption of Co on Pt(111) led to a localized reconstruction of the Pt(111) substrate; and at the same time the reconstructed areas of the substrate resulted in a self-assembled growth of Co overlayer.[7,8] Long-range electrostatic, magnetic, or elastic interactions are probably responsible for spontaneous formation of domain structures, which have been observed or predicted in two-dimensional (2D) systems.[9]

Recently, we have studied the growth, structure, and thermal properties of metal chromium films deposited on Pt(111).[10,11] Within the first two monolayers (ML), Cr grows pseudomorphic to the substrate Pt(111) surface at room temperature. The film is under a nonisotropic strain, compressed 4% and extended 10% along the two directions of the hexagonal unit cell, respectively. After annealing various Cr overlayer coverages to different temperatures, metastable surface alloys typical of a miscible metallic system have been observed. A highly ordered hexagonal pattern appears for a limited coverage range from 1.5–3.0 ML and an annealing temperature of 800 K. Its special nucleation site, high symmetry, and small periodicity, as well as the strong sensitivity of scanning tunneling microscope images to bias voltage, reveal remarkable characteristics for the process of self-organization on Pt(111). We have attributed the results to a structural manifestation of strong strain relief formed by deposition and annealing of a chromium overlayer on the Pt(111) surface as discussed recently.[12] In this paper, we cover the experimental results in detail and present calculation results on the electronic structure of the Cr/Pt(111) system based on density-functional theory within the local spin-density approximation.

II. EXPERIMENT AND COMPUTATION

A. Experimental procedure

The experiments were conducted in an ultrahigh vacuum (UHV) system operating at a base pressure of 5×10^{-11} mbar. The system is equipped with capabilities for x-ray photoelectron spectroscopy (XPS), low-energy He+ ion scattering spectroscopy (ISS), low-energy electron diffraction (LEED), and scanning tunneling microscopy (STM) measurements.[10]

Chromium overlayers were prepared by vapor deposition of Cr on a clean Pt(111) surface at room temperature in UHV. Afterwards, the samples were annealed to certain temperatures and quenched down to room temperature for various measurements. The Pt(111) single crystal employed was a 8 mm-diameter disk, with a thickness of 1 mm. The crystal has been oriented by Laue diffraction within 0.5° of the (111) orientation and mechanically polished. The surface was cleaned by 1 keV argon ion sputtering at room temperature for 30 min, followed by high-temperature sputtering at 900 K also for 30 min, then flashing in UHV at 1000 K for 5 min. After the procedure, the substrate was determined to be clean, since no contamination could be detected by XPS and ISS. LEED showed a hexagonal pattern with sharp points and very low background; STM showed clean and flat terraces with widths from less than 100 Å to several hundred Å. The chromium source consisted of a water-cooled evaporator, with a high purity (99.99%) Cr block about $5 \times 3 \times 2$ mm^3 in size clamped onto a *W* wire filament, which was resistively heated. To eliminate impurities, the evaporator was carefully outgassed. The sample temperature was measured using a *K*-type thermocouple mounted on the sample holder, calibrated to account for a gradient from the sample

to the actual point of temperature measurement. The coverage of chromium films was monitored by a quartz crystal microbalance. For convenience, the Cr coverage is converted to monolayers (ML), where 1 ML corresponds to 1.51×10^{15} Cr atoms/cm^2, the density of a Pt(111) surface. Typically, the evaporation rate was on the order of 0.05 ML/min.

The STM data were recorded in constant-current mode. Chemically etched tungsten tips, with no further treatment except for high voltage/high current pulses during scanning, were employed. The bias voltage was between -3.0 and $+3.0$ V, tunneling currents between 0.5 and 2.0 nA. The constant-current topographies (CCT) are shown in a top view representation, where brighter areas correspond to higher STM z values.

B. Calculation method

The electronic structure calculations were performed with the linear muffin-tin orbital method in the atomic sphere approximation (LMTO-ASA).[13] Exchange and correlation effects are treated within the local spin-density approximation (LSDA) of density-functional theory.[14] Self-consistent solutions to the Kohn-Sham equations are obtained for all electrons in the system using the exchange-correlation potential as parameterized by von Barth and Hedin.[15] The core electron states are solutions of the single-particle Dirac equation. Scalar relativistic terms are included in the Hamiltonian for the valence and conduction bands. The LMTO basis set included $4s$-, $4p$-, and $3d$-type functions for Cr $6s$-, $5p$-, and $5d$-type functions for Pt, and $1s$-, $2p$-, and $3d$-type functions for empty spheres. Pivotal energies on each site were chosen at the center of gravity of the occupied partial density of states. Only the $3d$-type functions on the empty spheres were linearized about the center of the canonical d band.

The atomic structure of the Cr/Pt system is based on the recently proposed model for the Cr-induced reconstruction of Pt(111) surface.[12] Because of limitations in computing time, a simplified structure (Fig. 8) that reflects the main features of the realistic model (Fig. 11) was used. Two kinds of supercells containing 78 lattice points were considered: (i) the PtCr unit cell as displayed in Fig. 8, alternating with layers of empty spheres (single layer super cell), and (ii) the PtCr unit cell alternating with layers of Pt atoms (sandwich super cell). In all, there are 28 different types of atoms in the unit cell. The irreducible wedge of the Brillouin zone was sampled with a set of 54 special k points. At self-consistency, convergence of the total energy was of the order of 10 meV.

III. RESULTS

A. STM results

STM images of Fig. 1 show the morphological changes of a 2.75 ML Cr film on Pt(111) surface before and after annealing at different temperatures. Figure 1(a) was obtained on the as-deposited film. Chromium grows mainly in two dimensions on the Pt(111) surface at a coverage below 2 ML.[10] At a coverage of 2.75 ML, the growth starts to become three-dimensional and Cr islands appear in some areas. After annealing at 600 K for 30 min, there is a general smoothening of the surface [Fig. 1(b)]. Most of the initially

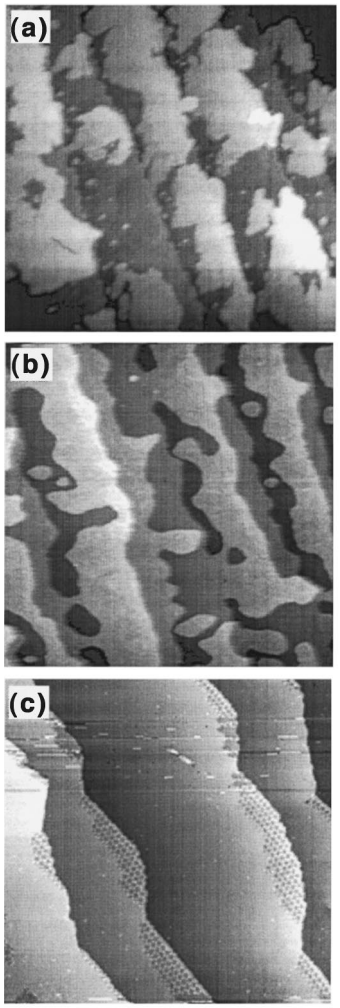

FIG. 1. STM images (900×900 Å^2) of a 2.75 MI Cr overlayer on Pt(111). (a) Image obtained after preparing the Cr film at room temperature ($V_s = +0.6$ V, $I_t = 0.6$ nA); (b) after annealing at 600 K for 30 min in UHV; some intermixing between the overlayer and the substrate takes place ($V_s = +0.7$ V, $I_t = 0.6$ nA); (c) after further annealing at 800 K for 30 min. Note the superstructure near the step edges ($V_s = +2$ V, $I_t = 0.6$ nA).

isolated islands disappear forming continuous areas with round edges; some lower-lying areas exist, largely at the areas that had no Cr islands before the annealing. This indicates that at this stage there is appreciable mass transport between the top layer and the ones underneath, that is, the intermixing of the overlayer Cr and the substrate Pt already takes place. This is further confirmed by the ISS, XPS, and LEED results described in following. Further annealing the Cr film at 800 K changes the overall surface morphology considerably and leads to flat surfaces that resemble a clean Pt(111) surface after sputtering and annealing to the same temperature. At the same time, however, spatial self-organization takes place at some areas, forming a nanoscale pattern as revealed in Fig. 1(c). In this image, there are five flat terraces with atomic steps of 2.3 ± 0.1 Å close to the value of clean Pt(111) surfaces (2.26 Å).[16] In addition, a reconstruction composed of ordered patches is seen near the descending steps. In most cases, the patches form long and narrow stripes parallel to the step edges.

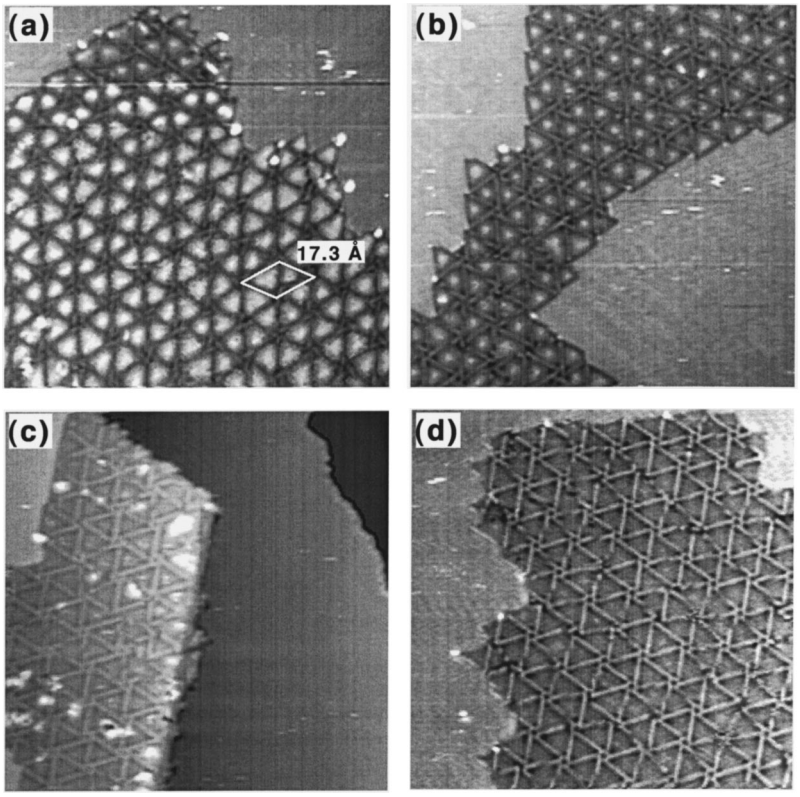

FIG. 2. High-resolution STM images (180×180 Å^2) of the reconstructed areas, showing a strong bias dependence of the contrast. Images are recorded with (a) $V_s=+2.0$ V, $I_t=0.6$ nA, showing a mosaic pattern with a hexagonal symmetry; (b) $V_s=+0.5$ V, $I_t=0.6$ nA, a network and the mosaic are seen simultaneously; (c) $V_s=-1.0$ V, $I_t=0.6$ nA, the contrast of the mosaic is much weaker, and the network stronger; (d) $V_s=-2.0$ V, $I_t=0.6$ nA, showing a hexagonal ''wagon-wheel'' network.

In Fig. 2 are shown small-scale STM images of reconstructed areas. Figure 2(a), which was recorded at a sample bias voltage of +2.0 eV, reveals a mosaic pattern with a hexagonal symmetry. The dimension of the unit cell of this superstructure is 17.3 ± 0.2 Å. The elements (white) of the mosaic have a triangular shape. A line profile indicates that the mosaic has a corrugation about 1.2 Å,[12] and the highest areas protrude above the surrounding flat, unreconstructed areas by 0.5 Å. At +2.0 V sample bias, STM always shows such a mosaic pattern, although the maximum z amplitudes vary within ±0.1 Å for different images. An image with a sample bias voltage of +0.5 V is shown in Fig. 2(b). The brightness of the mosaic decreases, and a network between the triangular elements of the mosaic appears. The boundaries between the reconstructed and unreconstructed areas are quite sharp, with a sawtoothlike shape as dictated by the network. Figure 2(c) shows an STM image of a different area, which was recorded at a sample bias voltage of −1.0 V. The image covers three successive terraces; the black terrace (upper right) is the lowest one. The reconstructed area and the brightest unreconstructed area (upper left) belong to a same terrace. The reconstruction always appears next to step edges of the terraces. [The images in Figs. 2(a), 2(b), and 2(d) show only parts of reconstructed areas, which again terminate at step edges.] However, some parts of the step edges are not reconstructed, as seen in Fig. 2(c). Compared to Fig. 2(b), the contrasts of the mosaic and the network change further in Fig. 2(c), with the elements of the mosaic almost at the same gray scale (z height) as the network. The randomly distributed bright spots in this image are possibly adsorbates. An STM image with sample bias voltage of −2.0 V is shown in Fig. 2(d). Here the elements of the mosaic [white in Fig. 2(a)] disappear completely, and a ''wagon-wheel'' network composed of triangular spokes dominates. Line profiles show that the network is lower than the flat, unreconstructed parts of the same terrace and that it has a corrugation of 0.4 Å.[12] The wall width of the network is 2.6 Å, approximately one atom wide. Note that the edges of triangles in the network do not connect to a point, but the ends form a small ring in the center. The network possesses the symmetry of the two-dimensional space group $p6$. No preference for left or right rotations is observed, for example, the structures are left handed in Figs. 2(b) and 2(d), and right handed in Fig. 2(c), respectively. Independent of the bias voltage, the center always appears as a void. There are some defects in the network, indicating that it is stable against local imperfections. Within the typical bias voltages (−2.0 to +2.0 V), the observed z heights of the elements of the mosaic change dramatically with respect to the unreconstructed areas. The network changes very little. In fact, the network is even seen faintly between the elements of the mosaic in image Fig. 2(a).

This strong contrast sensitivity on the bias voltage is further displayed in Fig. 3, in which the STM sample bias voltage is increased successively in steps of 0.5 V from −2.0 V in the lower part to +2.0 V in the upper part. Figure 3(b) is after a background compensation of the raw STM image [Fig. 3(a)]. The different z heights in the raw image are at-

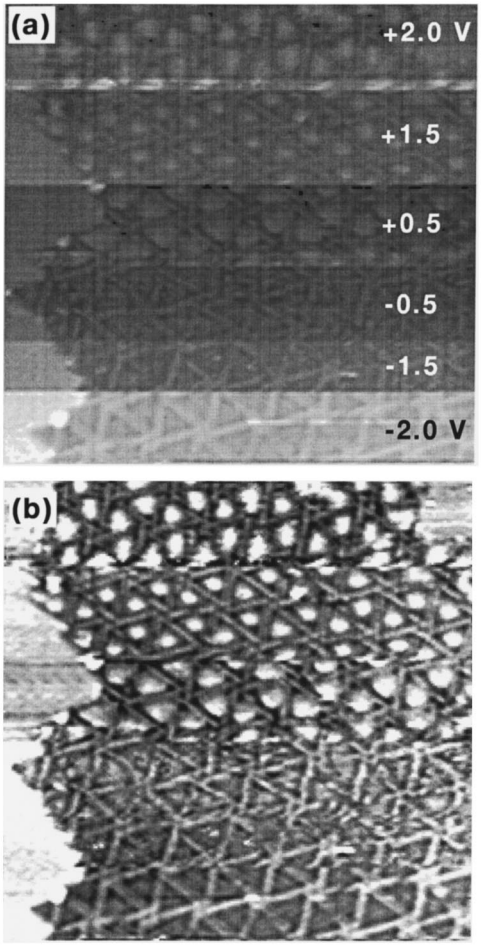

FIG. 3. STM image (160×160 Å^2) of a reconstructed region, displaying a strong bias dependence. (a) A raw image taken with various sample bias voltages as indicated; (b) after a line-by-line background compensation of image (a).

tributed to jumps of the tip when bias voltage is changed suddenly. When the voltage is stepped up, the ''wagon-wheel'' network [Fig. 2(d)] appears first. The most dramatic change occurs when the polarity of the sample voltage is reversed (at $+0.5$ V), when the bright elements of the mosaic suddenly appear. They gradually change in contrast until the elements protrude above their surroundings, similar to Fig. 2(a). Note that this image has been obtained on the same area as Fig. 2(d) where the whole image displays the network. (The area can be identified by the overall shape of the reconstructed region, as well as several white clusters at the left boundary to the unreconstructed area.) The STM contrast change displayed in Figs. 2 and 3 is highly reproducible, although sometimes the relative z amplitudes differed from the ones shown here.

STM images are quite stable when scanning the reconstructed areas with bias voltages within ±2.0 V. However, the STM tends to damage the surface when a voltage higher than 3.0 V is used. Figure 4 shows an STM image that was recorded with bias voltage of 2.0 V. The same area had previously been scanned with an STM sample bias voltage of 3.0 V. Some of the bright elements appear to be dislocated from their proper positions, forming a more disordered mosaic pattern, but the network remains almost intact. An enlargement is shown in the inset. We suggest that the white elements can be moved to some extent in the strong field of the STM tip. (One should also consider that some of the bright elements in Fig. 4 could stem from field-induced deposition of tip material. We think that this is less likely in this case, since no additional clusters appear on the flat, unreconstructed areas, which were scanned with a sample voltage of 3.0 V as well.) A movement of the mosaic elements by the STM tip would suggest that they are related to a physical arrangement of atoms, not solely a change in the electronic structure. They must be physically different from the more stable network. Tip-induced mobility may possibly be the cause for the observation presented in Fig. 5. Two triangular pits, with sizes corresponding to the triangles of the network, are shown. Several clusters have been seen close by, possibly coming from the pit areas. As revealed by a line profile, the pits have a flat bottom and a depth of about 1.4 Å.

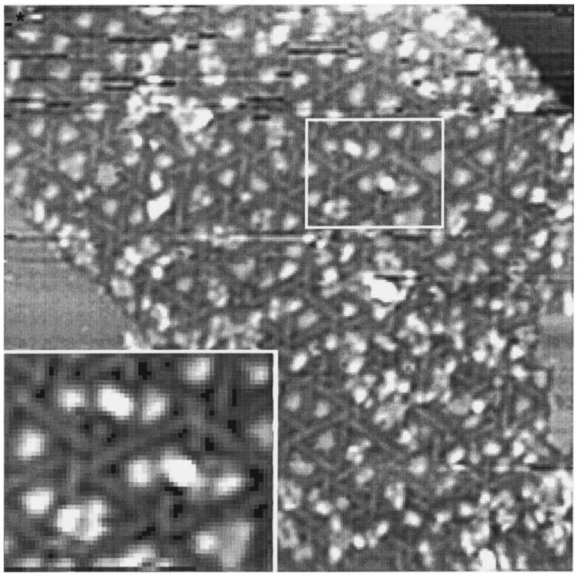

FIG. 4. STM image taken on an area that had been scanned previously with an STM sample bias voltage of $+3.0$ V ($V_s=+2.0$ V, $I_t=0.6$ nA, 180×180 Å^2). The white elements of the mosaic pattern appear dislocated from their regular positions during the previous high-voltage scan. The inset shows an enlargement of the small area indicated by the box.

The contrast of STM images is a convolution of the electronic states of sample and tip. A change in tip shape or composition may alter the appearance of images dramatically. As shown in Fig. 6 tip-related effects are also seen occasionally in this system. Figure 6(a) shows triple features, that is, every element of the mosaic is not a single triangle, but consists of three smaller elements. The elements are about 0.5 Å higher than their surroundings, which is typical for a sample bias of $+2.0$ V. We attribute the appearance to a triple tip, i.e., not one atom but three atoms form the apex of the tip. Another observation is shown in Fig. 6(b), where a stronger corrugation of the mosaic pattern is seen. Its appearance compares with the mosaic pattern shown in Fig. 2(a), except the amplitude of the white triangles is higher here (0.7 Å above the unreconstructed area), and the spacing between these triangles is much smaller. This figure is a part of a larger image, where the first part suffered from a loss in

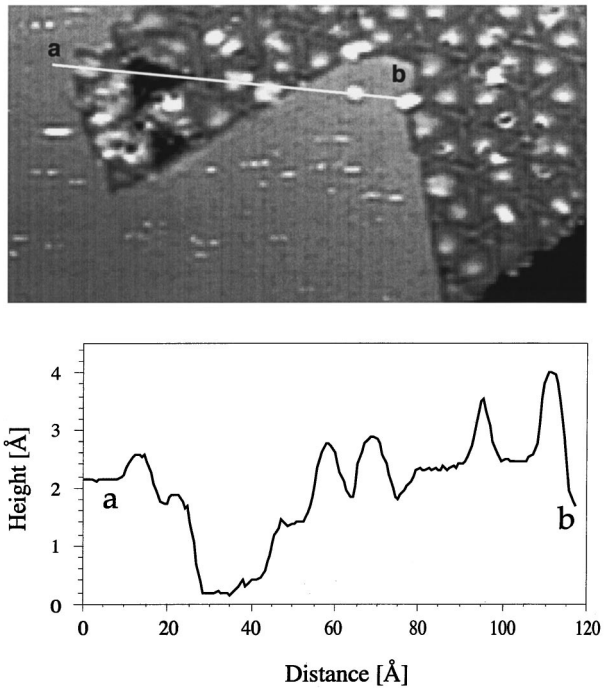

FIG. 5. STM image showing triangularly shaped holes in a reconstructed area. A related line profile is also shown (180×90 Å^2 $+1.0$ V, 0.6 nA).

resolution. Therefore, we speculate that it was a tip change that was responsible for this contrast change.

B. ISS, XPS, and LEED results

Figure 7 shows three ISS spectra that correspond to Fig. 1, respectively. Spectrum (a) was taken just after the deposition of the overlayer. A large chromium signal and a small platinum signal indicate that with a nominal coverage of 2.75 ML most of the Pt(111) surface is covered by the chromium overlayer. (The small peak to the right of the Pt position is caused by the nonmonochromatic ion beam of our setup.) The first two monolayers of Cr essentially wet the Pt substrate although not completely,[10] consistent with the STM observations described above. After annealing at a temperature of 600 K, however, the signal of Cr decreases, and the Pt peak grows dramatically as seen in spectrum (b), reflecting the interdiffusion of the two metals. Further annealing at 800 K results in a Pt signal increase to almost the intensity of a clean Pt(111) surface. Although the majority of Cr atoms have diffused into the substrate, some Cr still exist on the Pt surface as revealed by a small peak, which matches a Cr coverage of about 0.15 ML. No other species have been observed except for some oxygen that was occasionally detected after prolonged STM measurements. For different experiments, the Cr ISS intensity corresponds to the area covered by the superstructure as shown in the STM image of Fig. 1(c).

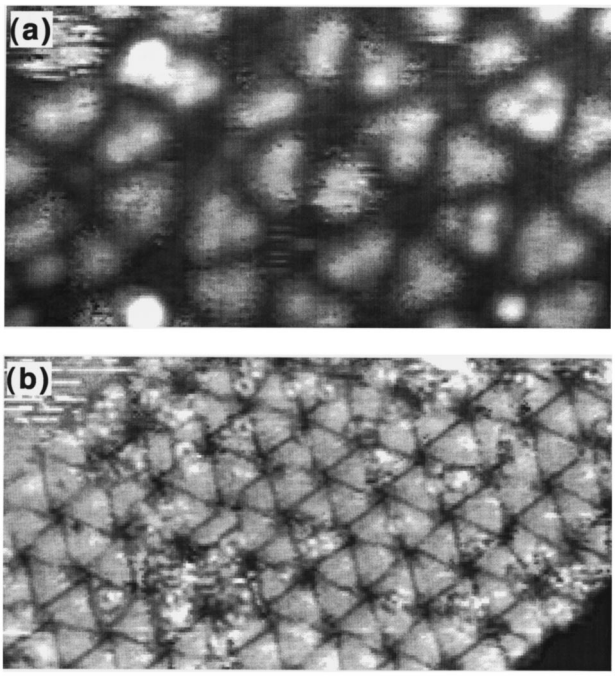

FIG. 6. STM images showing tip effects (see text). (a) 45×25 Å^2; (b) 180×90 Å^2. For both images $V_s=+2.0$ V, $I_t=0.6$ nA.

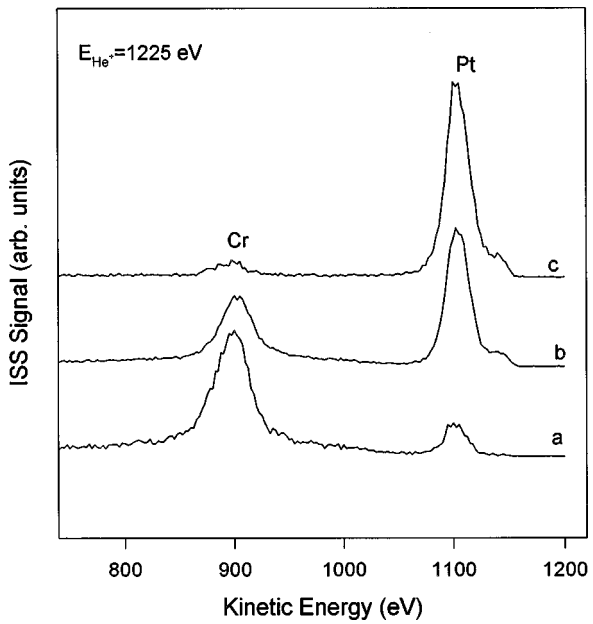

FIG. 7. ISS spectra of 2.75 ML Cr film on Pt(111). (a) Taken from the as-deposited overlayer; (b) after annealing at 600 K; (c) after annealing at 800 K.

The XPS and LEED observations correlate closely with the results of STM and ISS. For the first stage as shown in Fig. 1(a) and the spectrum (a) of Fig. 7, the Cr $2_{p3/2}$ core-level position (574.2 eV) is slightly lower than the one of a thick overlayer of 10 ML (574.4 eV).[10] Because of the complexity of the electronic structures of these two transition metals, the small shift of Cr binding energy does not rule out strong interactions between the overlayer and the substrate.[10,11] LEED shows a hexagonal (1×1) pattern of a clean fcc Pt(111) surface with smeared-out satellite spots. The Cr overlayer is mostly pseudomorphic to the Pt(111) surface, in addition, growth of a phase with a bcc (110) orientation starts already at this coverage.[10] No long-range reconstruction occurs at room temperature. After annealing at 600 K, the intensity of the Cr $2p$ core levels is attenuated

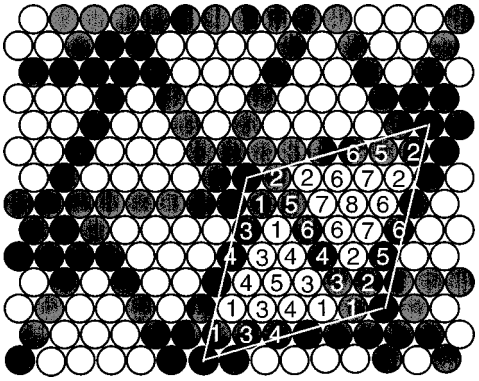

FIG. 8. Simplified structural model of a realistic structure (Fig. 11). The labeled numbers indicate the positions with different environment. Gray circles, Pt atoms; white circles, Cr atoms. At the corners of the unit cell are void sites.

greatly, but there is no obvious change in binding energy within the error bar (± 0.2 eV). In LEED, the intensity of the main spots decreases, and satellite spots disappear, indicative of Cr migrating into the Pt substrate and the formation of an ordered Cr-Pt alloy. Finally, the Cr XPS signals almost disappear after annealing at 800 K. In view of the large sampling depth of XPS ($\sim$20 Å), this result indicates that the Cr concentration in the near-surface region is very low. LEED measurements show that, except for the sharper (1×1) spots, six ill-defined, weak satellite spots appear. Probably, the area covered by the hexagonal superstructure [Figs. 1(c) and 2] is too small to give rise to a distinct LEED pattern.

C. Calculation results

A possible interpretation of the experimental results presented in Secs. III A and III B is a superstructure consisting of an ordered array of small Cr clusters separated by lines of Pt atoms. A detail discussion of the geometry and the formation mechanism of such a structure is given in the next section. Because of limitations in computing time, we have performed electronic structure calculations of a simplified model of an alloy (see Fig. 8) that reflects the main features of the ''real'' bimetallic structure.

The electronic properties of transition metals are dominated by narrow conduction bands formed from the overlap of fairly localized *d* orbitals.[17] As revealed in our calculation of the local density of state (LDOS) of a Cr surface, the contribution from *s* and *p* orbitals is one order of magnitude smaller than that from *d* orbitals. Therefore, only the *d* states of Cr are presented in the following. For the more noble metal Pt the LDOS is a sum of the related *s*, *p*, and *d* states.

The LDOS based on the simplified model of the Cr-Pt superstructure (Fig. 8), separated by vacuum layers (single layer super cell), is shown in Fig. 9. In Fig. 9(a), the LDOS of the Pt atoms, which are related to the Pt positions 1 and 5 in Fig. 8, are given, respectively. These two bands have similar shape, but peak at different energies, with the curve of Pt position 5 shifted to lower energy by 1.8 eV. The common feature is that the bands are almost completely situated below the Fermi level, with a width of about 4 eV. In contrast, the bands of Cr are mainly concentrated above the Fermi level [Fig. 9(b)], and are narrower as compared to Pt. As

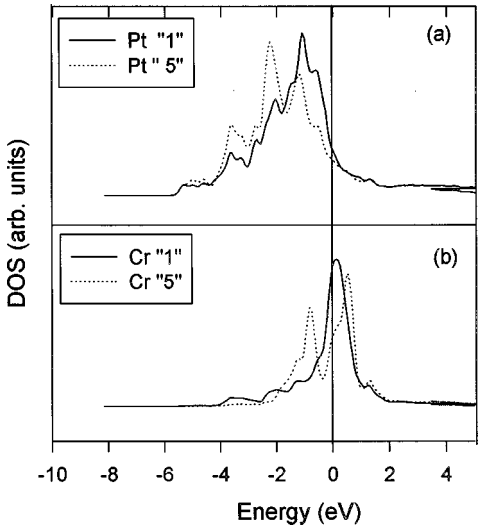

FIG. 9. LDOS calculated for Cr and Pt atoms at different positions within a single layer super cell of the simplified structure (Fig. 8).

seen in Fig. 9(b), there are two peaks in the curve of Cr position 5. The main peak is located at 0.7 eV above the Fermi level. For Cr position 1, the peak moves to lower energy, but is still centered above the Fermi level. There are eight different local environments for Cr atoms (see the labeled numbers in the model in Fig. 8), however, the calculation shows great similarity for the following positions: 1 and 2; 3, 4, 6, and 7; as well as 5 and 8. The biggest difference is between position 1 and position 5, which is shown here.

The LDOS of the surface unit cell sandwiched between layers of pure Pt is shown in Fig. 10. When comparing Fig. 9(b) with 10(b), it is seen that the basic features of Cr LDOS (shape, width, and peak position) remain similar. For Pt atoms in Fig. 10(a), the general distribution of the LDOS is still concentrated largely below the Fermi level. However, the distribution of the densities of states is broader than is the

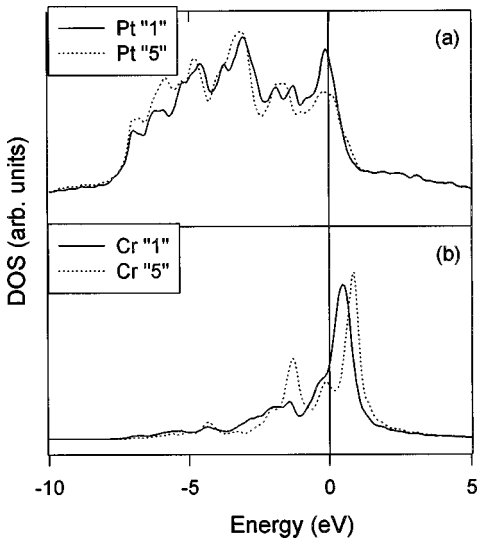

FIG. 10. LDOS calculated for Cr and Pt atoms at different positions within a super cell of the simplified structure (Fig. 8) sandwiched between Pt layers.

case for the single layers [Fig. 9(a)]. This difference corresponds to the removal of a large number of metallic bonds (six per atom) above and below the single layer. The ''real'' case supposedly lies between these two extremes; with vacuum above the mixed PtCr layer, but an infinite stack of Pt layers underneath. Although these calculations neglect many features of the real geometric structure, they nevertheless allow to draw a general conclusion: above the Fermi level, the LDOS is dominated by Cr states, while the LDOS of the Pt atoms is mainly located below the Fermi level.

IV. DISCUSSION

A. Chemical composition of the superstructure

We first address the chemical composition of the reconstructed areas. Generally speaking, it can be considered as a Cr-Pt alloy. The STM images of Fig. 1 and the ISS results of Fig. 7, as well as XPS and LEED observations, indicate clearly that annealing induces interdiffusion between the overlayer Cr and the substrate Pt. Cr and Pt atoms mix uniformly in the bulk.[18] However, it is not immediately obvious how to identify the composition of the small domains of the highly ordered superstructure.

It is instructive to draw a comparison between the Cr/Pt(111) and Ag/Pt(111) systems, because STM images show, to some extent, a similar appearance for both systems. Ag and Pt atoms are immiscible in the bulk. At submonolayers, a strained bimetallic alloy can be formed.[19] Annealing to 750 K leads to complete intermixing of Ag and Pt, but only in the top layer. For a higher thicknesses of the Ag overlayers, a reconstruction in the second monolayer occurs, first forming a metastable striped incommensurate phase and then converting into a trigonal network of domain walls upon annealing.[20] For Cr/Pt(111), the superstructure has been observed only for Cr overlayers with nominal coverage in the range of 1.5–3.0 ML, and after annealing at a temperature of 800 K. ISS and XPS indicate that most atoms of the Cr overlayer diffuse into deeper layers. The ISS signal of Cr as presented in Fig. 7(c) is proportional to the reconstructed areas for different experiments. Because of the pronounced intermixing in the bulk, we believe that both Pt and Cr are involved in the reconstruction.

Next, we discuss the locations of the Cr and Pt atoms in the reconstructed areas. The network in Fig. 2(d) reminds of the reconstructions observed on Au(111),[21] as well as on Pt(111),[22] which consist of domains of hcp- and fcc-stacked atoms separated by dislocation lines. On Na-covered Au(111), the domain structure has hexagonal symmetry and is poorly ordered when the Na coverages exceed 0.2 ML. In the presence of supersaturated platinum vapor, the Pt(111) surface reconstructs to form a network with a single orientation domain at 600 K. It seems reasonable to explain the network in Fig. 2(d) by invoking a similar reconstruction of the top-most layer of Pt(111). However, one remarkable novel feature is the strong sensitivity of the STM images to the bias voltage in our case. Figures 2 and 3 show that with a sample bias voltage of -2.0 V, the STM images display a ''wagon-wheel'' network, and a mosaic pattern appears at $+2.0$ V. In between, the two textures display themselves simultaneously. Since the bias dependence of the STM images is highly controllable and reproducible, it is attributed to sample properties rather than tip effects.

To first order, the global features in constant-current STM images correspond to surface topography. Finer details in STM contours, such as surface corrugations, will undoubtedly display a combination of structural and electronic properties. On semiconductor surfaces, in particular, it is more appropriate to think of the STM as measuring surface electron wave functions instead of atom core position because of the localized states of these materials.[23] STM line profiles show that the height of the network appears lower than that of the unreconstructed areas of the same terraces, and has a corrugation of 0.4 Å, which does not change significantly with bias voltage. The wall width of the network is 2.6 Å, nearly one atom wide. But the contrast of the mosaic changes dramatically, with a corrugation of about 1.2 Å at $+2.0$ V sample voltage to almost zero at -2.0 V. It is obvious that strong electronic effects are involved. Considering that the elements of the mosaic appear to be physically affected by the STM tip at high bias voltages, but that the network is left intact (in Fig. 4), we believe the mosaic elements are composed of arrays of atoms, most likely consisting of Cr. The general conclusion reached from the electronic structure calculations, i.e., Pt and Cr atoms in very different environments still preserve the overall location of their LDOS below and above the Fermi level, respectively (Figs. 9 and 10) is in accord with this assumption. Compared to Pt, Cr has a higher unoccupied LDOS close to Fermi level, therefore Cr clusters will appear bright when imaged with positive STM sample bias voltages.

B. Structural model

The remarkable geometric configuration of the reconstruction itself, with one-atom-wide corrugation lines, highly ordered hexagonal symmetry, and a small unit cell ($a = 17.3$ Å), leads us to propose the atomistic model presented in Fig. 11. It is based on the above-mentioned features observed in other reconstructions of metal elements,[21,22,24–29] namely, domains of fcc- and hcp-stacked areas separated by dislocation lines. The smallest circles in Fig. 11 represent the top-most layer of the unreconstructed Pt(111) bulk. On top of this layer, Pt atoms sit either in fcc (gray) or in hcp (black) positions within triangular areas. A one-atom-wide boundary (light gray) separates these fcc and the hcp domains. Seven Pt atoms comprise this boundary. Five of the Pt atoms in one boundary are placed at bridge sites along the $\langle 110 \rangle$ directions. The two atoms at the ends are shifted slightly toward the center of the hexagon, to energetically more favorable positions. These bridge-bonded atoms must protrude above the platinum atoms in threefold fcc and hcp positions in the triangles.

It is unlikely that a Pt atom occupies the on-top site in the middle of the ring, otherwise it would exhibit a higher corrugation than the surrounding bridging Pt atoms and would be imaged white in Fig. 2(d). Experimentally, however, the center of the ring is always observed as a hole with a diameter of about 2.1 Å and a depth of 0.3 Å. The Cr atoms in the alternating triangles, i.e., the regions with fcc and hcp stacking, are connected by these corrugation lines, which are essentially lines of Shockley partial dislocations with Burgers

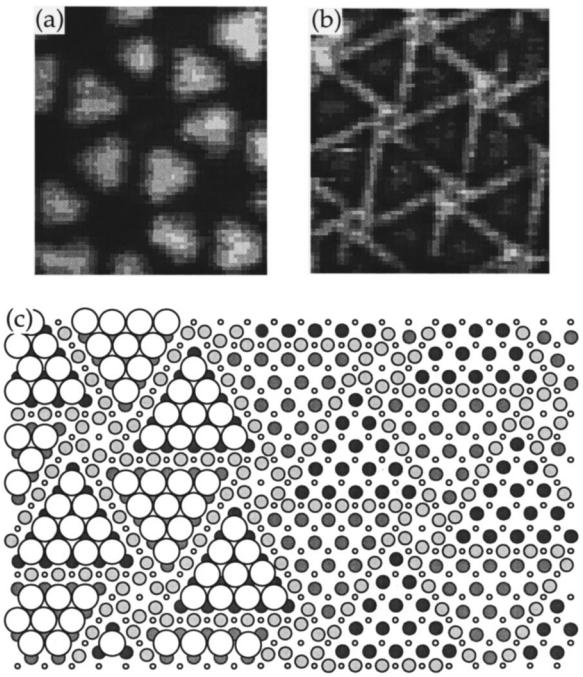

FIG. 11. A model for the Cr/Pt(111) reconstruction (c). The gray and black atoms show the close-packed fcc and hcp domains of the reconstructed Pt layer, respectively. The domains are separated by bridge-bonded Pt atoms (light gray). Small circles represent the Pt(111) layer underneath. On the left, top-layer Cr atoms are shown as big white circles. (a) and (b) are enlarged STM images corresponding to Figs. 2(a) and 2(d), respectively (40×40 Å^2).

vectors described as $b=(a/6)[1\bar{1}2]$ (Ref. 30) where a is the lattice constant of the Pt crystal. It is worthy to comment on two points. First, the corrugation lines along the close-packed ⟨110⟩ direction is an added atom line rather than a string of vacated sites. Classically, such a stacking fault is forbidden. Second, this dislocation has a mixed character with edge and screw components. In the model, the dislocation lines are oriented at an angle of 30° with respect to their Burgers vectors. Because of the hexagonal symmetry, the vector sum of the Burgers vectors within a local triangle is zero, which minimizes the energy. (The energy of a dislocation is proportional to the square of its Burgers vector.) Note that the ''wagon-wheel'' structure avoids a crossing of dislocation lines that would cost additional energy. Relative to unreconstructed Pt(111), the reconstruction forms a $\begin{bmatrix} 5 & 2 \\ -2 & 7 \end{bmatrix}$ network, i.e., a $(\sqrt{39}\times\sqrt{39})$R16.1° structure. The dimension (17.3 Å) and the rotation angle of the unit cell are in quantitative agreement with the experimental results.

It is known that the small energy difference between the two stacking types (fcc stacking has slightly lower energy compared to hcp) generally results in a unidirectional contraction and in larger fcc- than hcp-stacked areas.[21,24–29] Even for isotropic contractions, a deformation of the corrugation lines occurs favoring fcc stacking.[20,29,31] However, in our case the corrugation lines form a highly ordered hexagonal network with very small periodicity. Any deviation from this compact configuration will cost more energy than is gained by changing the stacking type, thus it is not unexpected that the triangles are equally sized. The model shown in Fig. 11 explains the dimensions and directions of the unit cell of the reconstructed surface, but interpretation of the vertical dimensions is complicated by electronic effects. Hence, we neglect the possible vertical relaxation of the second or even deeper Pt(111) layers in this model. Calculations using the embedded atom method show that in case of Ag adsorbed on Cu(111), the corrugation of the top Cu layer can be as large as 0.44 Å due to relaxations. Such large relaxations can influence as many as eight underlying layers.[32]

Compared to an unreconstructed Pt(111) surface, the atomic density of the reconstructed layer increases dramatically by 31% (51 top atoms compared to 39 in an unreconstructed surface if we count the higher lying Pt atoms in bridging position as part of the reconstructed layer). This reflects a general trend: the smaller the structure, the higher the atomic density. For the herringbone reconstruction on Au(111) and Pt(111) surfaces, the increase in surface density is about 4%, and the periodicities are almost one order of magnitude larger;[25,27] for the Na-induced distorted hexagonal Au(111) reconstruction, the values range from 6% to 9% and the dimensions of the hexagonal elements are 70–95 Å.[21] In this case, the increase in surface density is very large for a close-packed (111) surface, and caused by Pt atoms at bridge sites. It has been found that reconstructions of Ir, Pt, and Au(100) involve the formation of contracted and sometimes rotated hexagonal monolayers with a surface density of atoms increased by 20%, 23%, and 27.7%, respectively. Although the density of a (100) face itself is lower than that of a (111) face, these two cases are comparable as they result mainly from the registry involving bridge sites.[33]

C. Mechanism of the self-organization

It is well-known that the surfaces of Pt(111) and Au(111) will reconstruct at certain conditions to form various patterns, such as the well-known herringbone structure.[21,25–27] The general explanation of these phenomena is based on a theoretical study by Needs, Godfrey, and Mansfield.[34] Three effects are invoked to determine the stability of these surfaces: (1) Compared to the bulk, surface atoms have tendency to form shorter bond lengths because of the loss of symmetry, resulting in a higher density; (2) in order to increase its density, excess atoms have to be transferred into the surface layer, which costs extra energy; (3) the change of density leads to a partially incommensurate surface layer on the substrate, yielding mismatch energy. It is believed that (1) is the driving force of the reconstruction, while (2) and (3) tend to stabilize the unreconstructed surface.[26] In light of the similarity between the network observed here [Fig. 2(d)] and the ones formed by a Na-induced reconstruction on Au(111) (Ref. 21) and a supersaturated Pt gas-phase on Pt(111) at low temperature[26] it is straightforward to orient our interpretation on the same framework.

However, our findings exhibit significant new characteristics. First, the reconstruction involves Cr atoms, which form a highly ordered array of a two-dimensional clusters. For the miscible Cr/Pt system, especially after annealing at such a high temperature (800 K), a more uniform distribution of Cr atoms would be expected if the surface would simply reflect bulk phenomena. Second, the pattern formed is highly ordered, and the dimensions of the unit cell is relatively small (17.3 Å). In contrast, only a poorly ordered hexagonal network with a unit cell of about 100 Å has been observed

on Au(111) when the reconstruction is induced by alkali metals.[21] In the presence of a supersaturated Pt vapor, the network on Pt(111) has a similar quality as the one formed on Au(111).[22] Third, the step edges are the preferred zones for the Cr/Pt(111) reconstruction. There is certainly a difference of the stress fields between areas near step edges and areas in the middle terraces; and stress relief may play a role in the formation of the reconstruction.

We believe that Cr plays an important role in the process. Because of the chemical interaction and the large lattice mismatch between the Cr overlayer and the Pt substrate, the pseudomorphic Cr overlayer exerts a strong stress on the top Pt(111) layer, which alters the coupling to the Pt layers underneath, thereby increasing the tendency for reconstruction. The annealing temperature also plays a role. Most of the Cr atoms diffuse into the bulk, and Pt comes to the surface. Once a critical temperature (800 K) is reached, a self-organization and ordering of the nanostructure occurs. The top Pt layer engages in a reconstruction, forming the ''network'' and preventing further interdiffusion of Cr and Pt. This confines the Cr in a regular array of two-dimensional clusters. Conversely, this array stabilizes the network. This interplay between overlayer and substrate is consistent with a previous observation on Co/Pt(111), where Co adatoms induce a local reconstruction of the Pt substrate. The reconstruction affects the growth of Co films, resulting in a self-organized quasidentritic pattern.[7,8] Instead of Pt gas as the source for the extra atoms in Pt gas-induced reconstruction on Pt(111) (Refs. 22 and 26) in our case the extra atoms come from the bulk. Diffusing Cr atoms substitute some Pt atoms, and part of these Pt atoms come to the top Pt layer. The reconstruction increases the density of the top Pt layer, and this high density may be the reason why diffusion of Cr into the substrate is hindered at the reconstructed areas. This high density implies a higher strain within the layer. This may also be an explanation why the reconstructed areas appear only close to step edges, where strain can be relieved more easily. The holes in Fig. 5 may also be related to stress. Note that the holes appear in reconstructed areas farther away from step edges, which are surrounded on three sides by unreconstructed regions. Before the holes are formed, the accumulated strain is possibly quite strong. A perturbation, e.g., by the STM tip during scanning, may push out these atoms from this strained region. This would explain the clusters observed nearby.

Experimentally, as well as theoretically, it has been shown that metal atoms that sit on metal surfaces tend to form clusters. Except for chemical interactions, short-range attractive forces caused by strain effects play a role. Ten is one of the ''magic numbers'' for the number of atoms in such a cluster.[35–38] However, long-range forces of mutual repulsion exist between clusters, which causes them to be uniformly distributed and ordered.[9] Such a mechanism may display itself in the Cr/Pt system. The formation of ordered arrays of Cr clusters is also related to the nucleation of the Ni islands on the Au(111) surface at surface lattice dislocations induced by the ''herringbone'' reconstruction.[6] However, in contrast to Cr, Ni atoms do not cause a Au(111) reconstruction, they only nucleate passively at already formed dislocation sites.

V. SUMMARY

We have shown, through STM ISS, XPS, and LEED measurements, that after annealing Cr films on Pt(111) a self-organization of a highly ordered nanoscale superstructure takes place in this system through a stress-related reconstruction. Although Cr and Pt are easily miscible at elevated temperatures, diffusion of Cr atoms into the substrate is partially hindered by the reconstruction of the topmost Pt layer. Two driving forces, namely, chemical bonding between the Cr overlayer and Pt, as well as thermal annealing, act simultaneously and reinforce each other, resulting in the reconstruction. The small dimension of the hexagonal unit cell is directly correlated with the high atomic density of the reconstructed surface. The Pt reconstruction forms a template for two-dimensional Cr clusters containing only ten atoms. Our results further show that this phenomenon is universal, and can also be expected in other strongly interacting bimetallic systems, possibly spawning a novel class of surface phases.

The electronic structure computations using LDA gives a qualitative interpretation of the contrast sensitivity of STM images to the sample bias voltage. Compared to Pt, Cr has a high-unoccupied DOS close to the Fermi level, therefore it will appear bright in CCT's with positive STM bias voltages. The calculation is based on a simplified model of the configuration of Cr/Pt(111) observed in the experiments, and it cannot give information about the dynamics. It would be very interesting to simulate the dynamic process of the self-organization as this should provide new insights into similar but still unexplored systems.

ACKNOWLEDGMENTS

This work has been supported in part by LEQSF-EPSCoR, the Petroleum Research Fund, the Center for Photoinduced Processes (NSF-EPSCoR), and DoE-EPSCoR.

*Present address: Center for Nanomachined Surfaces and Chemical Engineering Department, University of Delaware, Newark, DE 19716-3110.

†Present address: Seagate Recording Heads, 7801 Computer Ave. S., Bloomington, MN 55435-5489.

‡Author to whom correspondence should be addressed. Electronic address: diebold@mailhost.tcs.tulane.edu

[1] J. H. Davies and A. R. Long, *Physics of Nanostructures* (SUSSP Publications, Edinburgh, 1992).

[2] X. Deng, B.-K. Yang, S. A. Hackney, M. Krishnamurthy, and D. R. M. Williams, Phys. Rev. Lett. **80**, 1022 (1998).

[3] C. Teichert, M. G. Lagally, L. J. Peticolas, J. C. Bean, and J. Tersoff, Phys. Rev. B **53**, 16 334 (1996).

[4] C. Tölkes, P. Zeppenfeld, M. A. Krzyzowski, R. David, and G. Comsa, Phys. Rev. B **55**, 13 932 (1997).

[5] B. Voigtländer, G. Meyer, and N. M. Amer, Phys. Rev. B **44**, 10 354 (1991).

[6] D. D. Chambliss, R. J. Wilson, and S. Chiang, Phys. Rev. Lett. **66**, 1721 (1991).

[7] P. Grütter and U. T. Dürig, Phys. Rev. B **49**, 2021 (1994).

[8] P. Grütter and U. T. Dürig, Surf. Sci. **337**, 147 (1995).
[9] K. Ng and D. Vanderbilt, Phys. Rev. B **56**, 10 544 (1997).
[10] L. Zhang, M. Kuhn, and U. Diebold, Surf. Sci. **371**, 223 (1997).
[11] L. Zhang, M. Kuhn, U. Diebold, and J. A. Rodriguez, J. Phys. Chem. B **101**, 4588 (1997).
[12] L. Zhang, J. van Ek, and U. Diebold, Phys. Rev. B **57**, R4285 (1998).
[13] O. K. Andersen, Phys. Rev. B **12**, 3060 (1975).
[14] W. Kohn and L. J. Sham, Phys. Rev. A **140**, A1133 (1965).
[15] U. von Barth and L. Hedin, J. Phys. C **5**, 1629 (1972).
[16] J. M. MacLaren, J. B. Pendry, P. J. Rous, D. K. Saldin, G. A. Somorjai, M. A. Van Hove, and D. D. Vvedensky, *Surface Crystallographic Information Service: A Handbook of Surface Structures* (Reidel, Dordrecht, 1987).
[17] A. Zangwill, *Physics at Surfaces* (Cambridge University, Cambridge, 1988).
[18] M. Hansen, *Constitution of Binary Alloys*, 2nd ed. (McGraw-Hill, New York, 1958).
[19] R. Schuster, H. Roder, K. Bromann, H. Brune, and K. Kern, Phys. Rev. B **54**, 13 476 (1996).
[20] H. Brune, H. Roder, C. Boragno, and K. Kern, Phys. Rev. B **49**, 2997 (1994).
[21] J. V. Barth, R. J. Behm, and G. Ertl, Surf. Sci. **302**, L319 (1994).
[22] M. Hohage, T. Michely, and G. Comsa, Surf. Sci. **337**, 249 (1995).
[23] J. A. Stroscio and W. J. Kaiser, *Scanning Tunneling Microscopy* (Academic, San Diego, 1993).
[24] J. V. Barth, H. Brune, G. Ertl, and R. J. Behm, Phys. Rev. B **42**, 9307 (1990).
[25] K. G. Huang, D. Gibbs, D. M. Zehner, A. R. Sandy, and S. G. J. Mochrie, Phys. Rev. Lett. **65**, 3313 (1990).
[26] M. Bott, M. Hohage, T. Michely, and G. Comsa, Phys. Rev. Lett. **70**, 1489 (1993).
[27] A. R. Sandy, S. G. J. Mochrie, D. M. Zehner, G. Grubel, K. G. Huang, and D. Gibbs, Phys. Rev. Lett. **68**, 2192 (1992).
[28] S. Narasimhan and D. Vanderbilt, Phys. Rev. Lett. **69**, 1564 (1992).
[29] C. B. Carter and R. Q. Hwang, Phys. Rev. B **51**, 4730 (1995).
[30] J. Weertman and J. R. Weertman, *Elementary Dislocation Theory* (Macmillan, New York, 1964).
[31] C. Gunther, J. Vrijmoeth, R. Q. Hwang, and R. J. Behm, Phys. Rev. Lett. **74**, 754 (1995).
[32] S. M. Foiles, Surf. Sci. **292**, 5 (1993).
[33] M. A. Van Hove, R. J. Koestner, P. C. Stair, J. P. Biberian, L. L. Kesmodel, I. Bartos, and G. A. Somorjai, Surf. Sci. **103**, 218 (1981).
[34] R. J. Needs, M. J. Godfrey, and M. Mansfield, Surf. Sci. **242**, 215 (1991).
[35] C. Massobrio and P. Blandin, Phys. Rev. B **47**, 13 687 (1993).
[36] H. Roder, R. Schuster, H. Brune, and K. Kern, Phys. Rev. Lett. **71**, 2086 (1993).
[37] J. Tersoff, Phys. Rev. Lett. **74**, 434 (1995).
[38] G. Rosenfeld, A. F. Becker, B. Poelsema, L. K. Verheij, and G. Comsa, Phys. Rev. Lett. **69**, 917 (1992).